International Journal of Heat and Mass Transfer 165 (2021) 120698

Contents lists available at ScienceDirect

International Journal of Heat and Mass Transfer

journal homepage: www.elsevier.com/locate/hmt

Local laminarization within the mild pressure gradient flow over the heated wall

A. Yu. Sakhnov

Kutateladze Institute of Thermophysics SB RAS, Lavrentyev Ave., 1, Novosibirsk, Russia

ARTICLE INFO

Article history:
Received 19 September 2020
Revised 3 November 2020
Accepted 5 November 2020
Available online 25 November 2020

Keywords:
Boundary layer
Heat transfer
Laminarization
Velocity overshoot
Numerical modeling
Mild pressure gradient

ABSTRACT

The paper presents a numerical modeling of an air boundary layer over a heated wall in the presence of a mild streamwise pressure gradient. The numerical model consists of the Prandtl equations, which describe the dynamic and thermal processes within the boundary layer, and the k-ω-γ turbulence model, which is able to reasonably simulate a laminar-turbulent transition as well as a suppression of turbulence. In some simulated cases we blocked the turbulence model to obtain parameters of exclusively laminar flow. Throughout, we applied finite-difference methods for solving the partial differential equations. The simulation demonstrated that a local laminarized area may occur near the wall under the considered conditions. When this laminarization occurs, the boundary layer consists of a near-wall laminar part and an outer turbulent one. Such character of the stream leads to levels of friction and heat transfer intermediate to laminar and turbulent flows at the same conditions.

1. Introduction

Laminarization was first observed in 1954 during experimental investigations of flows under the influence of a favorable pressure gradient [1–3]. The authors of these works showed that flow acceleration suppresses the turbulence and reverses the flow to a laminar regime.

Flow laminarization results from various physical conditions including flow acceleration, gas suction through a permeable wall, actions of magnetic fields on flows of electrically conductive liquid, and heating of the leading edge of the wall in a boundary layer [4,5]. A specific application of laminarization is to the design, and investigation of flows around airfoils, which utilize laminarization caused by favorable pressure gradients [6–9].

There are many parameters of pressure gradient and flow acceleration which were suggested to describe laminarization criterion [10,11]. Some of these parameters take into account flow geometry, characteristics of the main flow and characteristics of the boundary layer; other parameters take into consideration only flow geometry and characteristics of the main flow. Presently for flows in convergent channels, investigators often use the acceleration parameter suggested by Launder in 1964 [12]: $K = (\mu_e/\rho_e U_e^2) dU_e/dx$. The K parameter may be defined through channel geometry and main flow characteristics, or through the velocity distribution in the streamwise direction.

Through a rather simple analysis of the integral momentum equation for the turbulent boundary layer, Kays calculated $K = 3.55 \times 10^{-6}$ as the minimal value, at which the relaminarization is possible [13]. However, experimental works [14,15] authors obtained a slightly higher critical K value of 4×10^{-6}. Using direct numerical simulation Araya and Torres [16] noted that during flow laminarization with $K = 4 \times 10^{-6}$, thermal parameters are transformed in large time and in a distance scales than dynamic ones. Lushchik et al. [17] demonstrated that complete relaminarization is reached after a rather long time under a favorable pressure gradient with $K = 6 \times 10^{-6}$. Saltar and Araya [18] showed that a decrease of Reynolds shear stresses and kinetic energy of turbulence within an accelerated flow is one of the direct indicators of the laminarization.

Laminarization is also possible in a channel with strongly heated walls [19,20]. The high heat flux into the channel leads to flow acceleration and consequently to a decrease in the kinetic energy of turbulence. This was observed by Takagi et al. [21] in the local laminarization of flow in a burning open jet of hydrogen-nitrogen mixture. Significant suppression of turbulence took place in the part of flame with the highest temperature. Authors found a weak laminarization in the non-reacting cold jet.

Local suppression of turbulence was obtained within the turbulent flow of a concentric annulus with a rotating outer wall [22]. Moderate rotation rates led to a decrease of turbulence near the outer wall, while high rotation rates led to laminarization near the inner wall.

E-mail address: aleksei_sakhnov@mail.ru

https://doi.org/10.1016/j.ijheatmasstransfer.2020.120698
0017-9310/

Nomenclature

$\frac{c_f}{2} = \frac{\tau_w}{\rho_e U_e^2}$	skin-friction coefficient
c_p	gas specific heat at constant pressure [J/(kg deg)]
$K = \frac{\mu_e}{\rho_e U_e^2}\frac{dU_e}{dx}$	stream acceleration parameter
k_t	kinetic energy of turbulence
$k_t^+ = \frac{k_t}{\tau_w/\rho_w}$	dimensionless kinetic energy of turbulence
P	pressure [Pa]
$\mathrm{Pr} = \mu c_p/\lambda$	Prandtl number
q	heat flux [W/m^2]
$\mathrm{Re}_x = \rho_e U_e x/\mu_e$	Reynolds number, based on streamwise coordinate x
$\mathrm{Re}^{**} = \rho_e U_e \delta^{**}/\mu_e$	momentum thickness Reynolds number
$\mathrm{St} = \frac{q_w}{\rho_e U_e c_p \Delta T}$	thermal Stanton number
T	streamwise mean temperature in wall coordinates
$T^+ = (T_w - T)c_p\sqrt{\rho_w \tau_w}/q_w$	temperature
U, V	velocity components in the x, y directions respectively [m/s]
$U^+ = U/\sqrt{\tau_w/\rho_w}$	streamwise mean velocity in wall coordinates
x, y	streamwise and normal coordinates relative to surface [m]
$y^+ = y\sqrt{\rho_w \tau_w}/\mu_w$	wall normal coordinate

Greek symbols

α	the convergence angle of top plane of channel [degrees]
γ	intermittency factor
δ	thickness of hydrodynamic boundary layer [m], $U/U_e = 0.995$or1.005
$\delta^{**} = \int_0^\infty \frac{\rho U}{\rho_e U_e}(1 - \frac{U}{U_e})dy$	momentum thickness boundary layer [m]
λ	heat conductivity $[W/(m \cdot K)]$
μ	dynamic viscosity $[Pa \cdot s]$
ρ	density [kg/m^3]
$\tau_w = \mu_w(dU/dy)_w$	wall shear stress $[Pa]$
ω	modified rate of turbulence dissipation

Subscripts

0	flow quantities at the start of flow
e	flow quantities in external flow
max	flow quantities with maximum value within a cross-section
t	turbulent quantities
w	parameter at the wall

Shiibara et al. [23] found laminarization within the pulsating flow of a straight circular pipe. It was shown that turbulence is suppressed during the acceleration phase of flow pulsation, which decreases heat transfer temporarily. By selecting the frequency of pulsations, authors reached the increase of heat transfer despite the laminarization. From there, Mikheev et al. [24] showed that the kinetic energy of turbulence in the pulsating flow changes its magnitude more than five times, reaching a maximum in the flow deceleration phase.

During experiments with velocity profiles modified to have additional near-wall flow acceleration, Kühnen et al. [25] found that under certain conditions, complete flow laminarization could be achieved.

There are many flow conditions under which the streamwise velocity profile may have a maximal value located within the boundary layer. Such phenomenon is called velocity overshoot. It can occur under several different conditions: forced and mixed convection, heterogeneous injection, combustion, moving wall, pulsating flow, wall jet and others. Boyarshinov et al. [26] examined combustion of ethanol in the boundary layer with a favorable pressure gradient. For an acceleration parameter of $K = 1.9 \times 10^{-5}$ the velocity overshoot was 85% at $x = 0.32m$ from the leading edge. The authors showed that the combined influence of the chemical reaction and the flow acceleration leads to an increase of heat transfer. Also, Volchkov [27] suggested a formula to calculate the maximum velocity in an accelerated flow with combustion. In the paper [28] we demonstrated that the expression proposed by Volchkov can also be applied to a rough evaluation of the maximum velocity in a non-reacting accelerated flow over a heated wall. Also, that paper has a short review on flows with the velocity overshoot phenomenon.

In previous papers we considered the effect of gas properties on the overshoot [29], compared the evolution of the velocity maximum under the conditions of constant wall temperature, and constant heat flux through the wall [30] and investigated the behavior of the overshoot with foreign gas injection [31]. Initially, we planned to focus the present study on the behavior and characteristics of the velocity overshoot within the turbulent boundary layer. For this reason we choose the mild pressure gradient with $K = 3 \times 10^{-7}$ to avoid a laminarization. However, our numerical modeling showed a decrease of the kinetic energy of turbulence and flow laminarization at the certain conditions. In this paper we define the laminarization as a strong suppression of turbulence: when $k_t^+ < 1$, and the intermittency factor is of approximately zero value. We follow by W.M. Kays [32] for the definition of mild pressure gradient as a factor that is not able to laminarize the flow. In contrast, the strong pressure gradient leads to relaminarization. So, the present paper has the goal of considering the laminarization of a turbulent boundary layer with the presence of a mild streamwise pressure gradient and significant wall heating, while taking into account the interaction of turbulence and the velocity overshoot.

2. Flow configuration and modeling approach

We consider the air flow in a plane convergent channel where the acceleration parameter $K = (\mu_e/\rho_e U_e^2)dU_e/dx$ [32] is held constant over the entire channel length (Fig. 1). From the formula presented in Fig.1 we know that the acceleration parameter, K, in a real flow channel depends on the convergence angle of the top plane, the initial velocity, the height of the inlet section, and the gas properties. K allows for unification of a wide range of accelerated flows including huge and relatively small channels, as well as various gases and initial conditions. The sloped top wall of the channel was assumed to be located quite far from the lower channel wall, i.e. $h_0 \gg \delta$, this is so the analysis can be focused on the accelerated hydrodynamic, and thermal boundary layers developing over the bottom surface. Throughout, main flow quantities are designated by the subscript "e".

The temperature of the incoming flow is $T_0 = 300K$. The lower wall is divided into three parts. The initial part with $T_w = 301K$ provides quasi-isothermal conditions up to $\mathrm{Re}_x = 4.5 \times 10^5$. At the second part of the wall the temperature increases linearly from $301K$ to the temperature of the heated wall at $\mathrm{Re}_x \geq 5 \times 10^5$. Finally, the third part is the heated to a constant temperature, T_w, which is set for different flow cases.

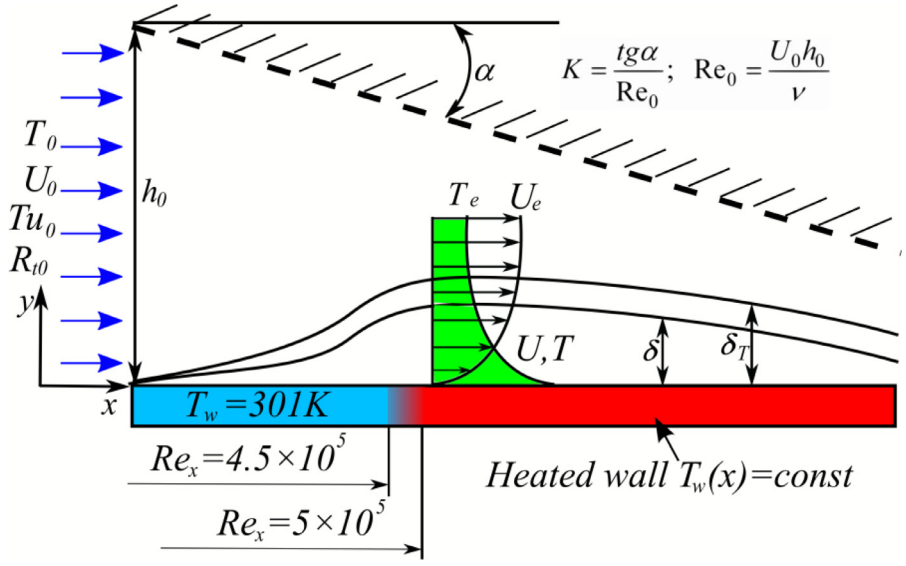

Fig. 1. Diagram of the flow considered.

2.1. Equations and boundary conditions

The flow considered can be well approximated by the parabolized two-dimensional momentum, continuity and energy equations for a steady boundary layer with variable gas properties:

$$\rho U\frac{\partial U}{\partial x}+\rho V\frac{\partial U}{\partial y}=\frac{-dP}{dx}+\frac{\partial}{\partial y}\left((\mu+\mu_t)\frac{\partial U}{\partial y}\right) \tag{1}$$

$$\frac{\partial(\rho U)}{\partial x}+\frac{\partial(\rho V)}{\partial y}=0 \tag{2}$$

$$c_p\rho U\frac{\partial T}{\partial x}+c_p\rho V\frac{\partial T}{\partial y}=\frac{\partial}{\partial y}\left(\left(\lambda+\frac{c_p\mu_t}{Pr_t}\right)\frac{\partial T}{\partial y}\right),\ Pr_t=0.9 \tag{3}$$

The fluid density is calculated from the ideal-gas state equation for the pointwise temperature and the ambient pressure $P=101kPa$. The properties of air at a point were determined from the polynomial dependencies involving coefficients taken from [33].

At the wall, the no-slip and constant temperature conditions were enforced:

$$y=0: U=0, V=0, T_w=const \tag{4}$$

At the outer edge of the boundary layer, the velocity U_e was determined by integrating the acceleration parameter $K=(\mu/\rho U_e^2)dU_e/dx$ while accounting for the variable viscosity and density of air, as well as the zero heat flux condition for the temperature field:

$$y\geq\delta: U=U_e=-\left(K\int_0^x\frac{\rho}{\mu}dx-1/U_0\right)^{-1},\ \frac{\partial T}{\partial y}=0 \tag{5}$$

The initial velocity of $U_0=5.2m/s$ was taken from the T3A experiment (ERCOFTAC)[34]. All flow cases were simulated at $\mathrm{Re}_x\leq 10^7$.

2.2. Turbulence model

In order to simulate the eddy viscosity μ_t used in Eqs. (1) and (3), we implemented Ge, Arolla and Durbin's [35] $k-\omega-\gamma$ turbulence model. This model can reasonably predict the laminar-turbulent transition with the intermittency factor γ. The model was adapted for the approximation of a boundary layer with variable gas properties with the following formulation:

The equation for kinetic energy of turbulence:

$$\rho U\frac{\partial k_t}{\partial x}+\rho V\frac{\partial k_t}{\partial y}=\rho P_k-C_\mu\rho k_t\omega+\frac{\partial}{\partial y}\left(\left(\mu+\frac{\mu_t}{\sigma_k}\right)\frac{\partial k_t}{\partial y}\right) \tag{6}$$

The equation for the specific dissipation rate of turbulence:

$$\rho U\frac{\partial \omega}{\partial x}+\rho V\frac{\partial \omega}{\partial y}=2\rho C_{\omega1}S^2-\rho C_{\omega2}\omega^2+\frac{\partial}{\partial y}\left(\left(\mu+\frac{\mu_t}{\sigma_\omega}\right)\frac{\partial \omega}{\partial y}\right) \tag{7}$$

The intermittency transport equation:

$$\rho U\frac{\partial \gamma}{\partial x}+\rho V\frac{\partial \gamma}{\partial y}=\frac{\partial}{\partial y}\left(\left(\frac{\mu}{\sigma_l}+\frac{\mu_t}{\sigma_\gamma}\right)\frac{\partial \gamma}{\partial y}\right)+\rho\left(P_\gamma-E_\gamma\right) \tag{8}$$

where $P_k=\gamma min(2\mu_tS^2/\rho,\ k_t|S|/\sqrt{3}),\ S=\sqrt{(0.5)}\partial U/\partial y$;

$P_\gamma=F_\gamma|\Omega|(\gamma_{max}-\gamma)\sqrt{\gamma}$,

$F_\gamma=2max[0,min(200-R_v,1)]\times min[max(R_v-R_{c,0}),4]$

$R_v=\frac{\rho d^2|\Omega|}{2.188\mu}$, d – distance to the wall;

$R_c=400-360min(T_\omega/2,\ 1),\ T_\omega=R_t|\Omega|/\omega, R_t=\mu_t/\mu$

$E_\gamma=G_\gamma F_{turb}|\Omega|\gamma^{1.5}$,

$G_\gamma=7.5max[0,min(100-R_v,1)]min[max(R_v-18,0),1]$,

$F_{turb}=exp\left(-(R_vR_t)^{1.2}\right)$

$\gamma_{max}=1.1$.

γ is redefined with every iteration using the following condition: $\gamma=min(\gamma,1)$.

For the boundary layer approximation we defined the vorticity as a derivative of streamwise velocity $|\Omega|=\partial U/\partial y$. Eddy viscosity was calculated with the following relation:

$$\mu_t=\rho k_t/\omega \tag{9}$$

The constants of the $k-\omega-\gamma$ turbulence model are presented in Tab. 1.

Table 1
Constants of $k-\omega-\gamma$ turbulence model.

C_μ	$C_{\omega1}$	$C_{\omega2}$	σ_k	σ_ω	σ_l	σ_γ
0.09	5/9	0.073	2	2	5	0.2

To solve differential equations (6) – (8), we set the following boundary conditions at the wall and in the main flow respectively:

$$\begin{aligned} y=0:\ & k_t=0,\ \omega=\frac{6\mu}{C_{\omega2}\rho y_1^2},\ \frac{\partial\gamma}{\partial y}=0 \\ y\geq\delta:\ & \frac{\partial k_t}{\partial y}=\frac{\partial\omega}{\partial y}=0,\ \gamma=1 \end{aligned} \tag{10}$$

Initial conditions were defined through the set turbulence intensity $Tu_0=\sqrt{2/3k_0}/U_0$ and turbulence scale $R_{t0}=\mu_t/\mu=\rho k_0/\omega_0\mu$ in oncoming flow. These parameters corresponded to the experiment ERCOFTAC T3A with $Tu_0=3.5\%$ and $R_{t0}=14$ [34].

2.3. Numerical method and testing

The system of time-independent differential equations described in parts 2.1 and 2.2 were solved by a finite difference method using a fully implicit scheme, which is well described in paragraph 7.3.3 of monograph [36]. The accuracy of the applied scheme was $o(\Delta x)+o(\Delta y)^2$. We used the Thomas algorithm to solve the derived system of linear algebraic equations. This algorithm was reported in paragraph 4.3.3 of [36]. Linearizing procedure was lagging the coefficients. The convergence criterion for the system of algebraic equations was $\varepsilon<10^{-5}$ with ε being the relative difference between the values of the required flow parameters at two sequential iterations.

The length of the wall was set to 7.72 m with the modeling area height of 0.5 m. We used an orthogonal computational grid with variable step sizes for both directions. The number of grid nodes normal to the surface was set 300 with grid compression coefficient $a=1.035$. As we demonstrated in paper [37], the grid compression coefficient a has more significant influence on the nodes' distribution within the boundary layer than the change of their number. To define the normal coordinate of the node j we used the following formula: $y_j=y_{j-1}+a^{j-2}\Delta y$.

Table 2
Magnitude of the grid step in streamwise direction for different Reynolds number ranges.

$\mathrm{Re}_x<100$	$100<\mathrm{Re}_x<10^7$
$\Delta x_0=8.75\times10^{-10}m$ $\Delta x_{\mathrm{Re}_x=100}=8.86\times10^{-7}m$	$\Delta x=2\times10^{-5}m$

Fig. 2a demonstrates results of the test on grid convergence. The test was done for the most extreme conditions of the considered flow. These conditions lead to the highest value of the velocity overshoot, which means an existence of the highest velocity gradients near the wall. As it is seen, the profile at $a=1.025$ differs noticeably from ones at $a=1.035$ and $a=1.045$. So, we applied $a=1.035$ for the further calculations. This coefficient a provides $y_1^+=0.07$ at $\mathrm{Re}_x=10^7$ and $T_w=301K$. It is the maximum value of the first wall coordinate among all flow cases considered in this paper. A decrease of Reynolds number and an increase of wall temperature lead to a decrease of the first wall coordinate.

Grid step, Δx, in the streamwise direction depends on the Reynolds number calculated with the streamwise coordinate, and the main flow velocity. Table 2 contains the minimal steps in the streamwise direction within certain ranges of Reynolds number.

Fig. 2b presents a comparison of experimental data with data simulated by the present numerical model. Black circles represent the T3A experiment (ERCOFTAC)[34] that has no pressure gradient in the streamwise direction. The simulation (line 2) of this experiment shows that the position of the transition to turbulence, and turbulent skin-friction coincide well with experimental values. Red triangles are the results of experiment 51468 carried out by Julien et al. [38]. The experimental channel had an initial length of 0.9144 m with zero-pressure gradient flow. For this reason, the simulated lines 2 and 4 coincide with each other up to $\mathrm{Re}_x\approx7\times10^5$. After the initial part the experimental setup had a convergent channel that formally provides the acceleration of $K=0.57\times10^{-6}$. The simulated skin-friction coefficient for the flow with this value of the acceleration parameter is slightly higher than the experimental

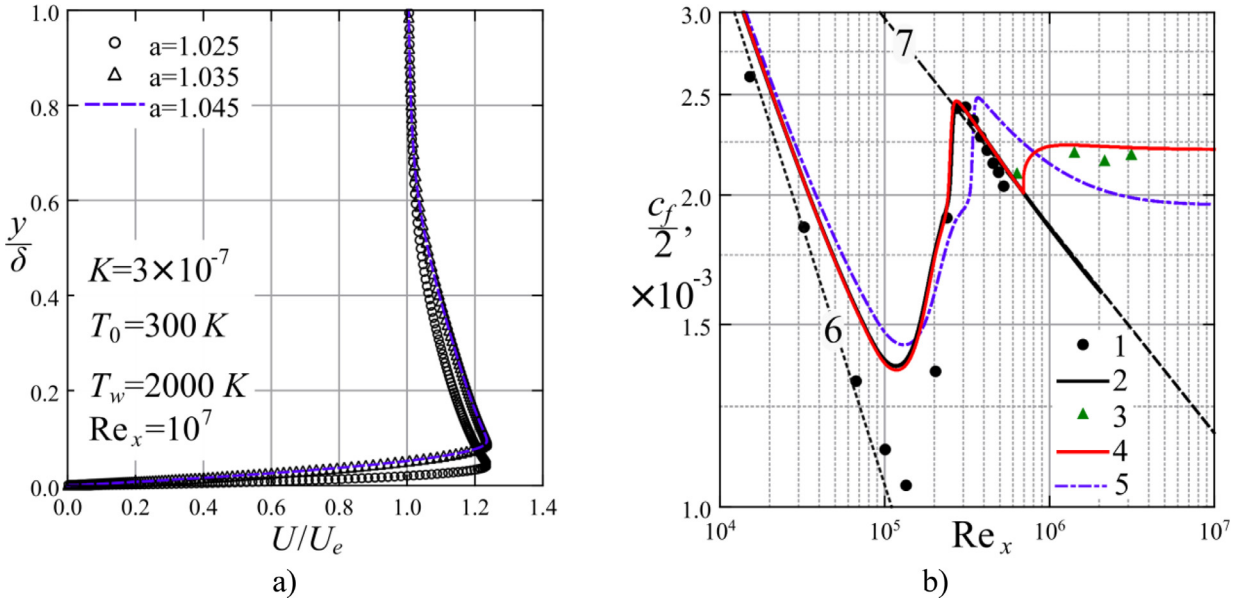

Fig. 2. Testing of the numerical model: a) test on grid convergence for velocity profiles; b) comparison of skin-friction coefficient with experimental data, 1 – experiment ERCOFTAC T3A [34], 2 – simulation of T3A flow, 3 – experiment for the flow with $K\approx0.57\times10^{-6}$ [38],
4 – simulation of the flow with $K=0.57\times10^{-6}$, 5 – simulation of the flow with $K=0.3\times10^{-6}$ considered in this paper, 6 – Blasius boundary layer $c_f=0.664\mathrm{Re}_x^{-0.5}$ [39],
7 – isothermal turbulent boundary layer with zero pressure gradient $c_f=0.059\mathrm{Re}_x^{-0.2}$ [39].

data. We explain this deviation by the lower real values of the acceleration parameter observed in the experiment. For instance, authors give $K = 0.55 \times 10^{-6}$ at the third point with $\mathrm{Re}_x \approx 2 \times 10^6$. Line 5 demonstrates skin-friction in the flow with $K = 0.3 \times 10^{-6}$ which we considered in this paper. Such acceleration has a noticeable effect on flow characteristics at $\mathrm{Re}_x > 10^6$.

3. Results

3.1. Boundary layer characteristics in streamwise direction

Fig. 3a presents dependencies of the skin-friction coefficient on Reynolds number. At $\mathrm{Re}_x < 4.5 \times 10^5$ all lines coincide with each other due to the same flow conditions. The favorable pressure gradient acting on the whole flow slightly delays the laminar-turbulent transition. Ghasemi et al. [40, 41] investigated the influence of pressure gradients on laminar, transitional and turbulent boundary layers. They confirmed by direct numerical simulation that acceleration leads to an increase of skin-friction coefficient for all regimes and to a delay of laminar-turbulent transition.

At the beginning of the heated section of wall the skin-friction coefficient drops in the flow-cases 2 – 6. This is explained by the decrease of the kinetic energy of turbulence (Fig. 4a). Below we will demonstrate that flows with $T_w[K] = 301, 500, 1100$ keeps the turbulent regime, and the local laminarization of the boundary layer takes place at $T_w[K] = 1110, 1500, 2000$. Dependencies 2 – 6 reaches a certain minimum and then increase. The reason for this increase is the occurence of the velocity overshoot (Figs. 6,7) in both regimes. In flow-cases 4 – 6 with the local laminarization the skin-friction coefficient is always lower than one in turbulent flows 1 – 3.

In order to demonstrate the budget of turbulence into the behavior of boundary layer we carried out the numerical modeling with a blocked turbulence model for $T_w[K] = 1110, 2000$. In these cases the skin-friction coefficient decreases at $\mathrm{Re}_x < 4.5 \times 10^5$ and increases significantly after the beginning of the heated wall. At $T_w = 1110K$ and $\mathrm{Re}_x = 3 \times 10^6$ skin-friction coefficients in the flows calculated with and without turbulence model (lines 4 and 7) almost coincide with each other though there is a certain tendency of deviation of these dependencies at $\mathrm{Re}_x = 10^7$. At the strong wall heating with $T_w = 2000K$ skin-friction coefficients in flows calculated with and without turbulence model (lines 6 and 8) are close to each other at $\mathrm{Re}_x = 10^6 - 3 \times 10^6$. With the increase of Reynolds number the skin-friction coefficient calculated with the blocked turbulence model exceeds the coefficient obtained with the working turbulence model. The reason of such behavior is the higher values of the maximal velocity (Fig. 6) within the laminar boundary layer than these ones in the boundary layer with the local laminarization calculated with a working turbulence model. It is worth noting that the skin-friction coefficient increases with the increase of wall temperature at any flow: turbulent, with local laminarization or laminar.

Fig. 3b shows dependencies of the thermal Stanton number on the integral Reynolds number. In [42] we demonstrated that when describing heat transfer in the flows with variable velocity of the main flow one has to use the integral Reynolds number that is $\mathrm{Re}_{\mathrm{int}} = \mathrm{Re}_L \int_0^{\bar{x}} U_e/U_0 d\bar{x}$, where $\bar{x} = x/L$, $\mathrm{Re}_L = \rho_e U_e L/\mu_e$ and L is the length of the wall. As it is seen, at ($\mathrm{Re}_{\mathrm{int}} > 4.6 \times 10^5$) Stanton number in turbulent flow (lines 1 – 3) on the heated wall decreases with the increase of Reynolds number and the increase of the wall temperature. This is the result of turbulence drop in the field of the heated wall (Fig. 4a).

Stanton number in the boundary layer with the local laminarization (lines 4 – 6) decreases with the increase of the integral Reynolds number and the wall temperature. It reaches almost the dependencies of Stanton number calculated with the blocked turbulence model (lines 7,8). However, Stanton number keeps an almost constant value with further increase of Reynolds number. At that, the increase of wall temperature increases Stanton number. It is worth noting that the transition to $\mathrm{St} = const$ coincides approximately with the arising of the velocity overshoot (Fig. 6).

Thus, heat transfer in the boundary layer with local laminarization is lower than one in the turbulent flow, but it is higher than one in absolutely laminar stream. Shome [43] obtained the similar situation within the turbulent flow in the asymmetrically heated horizontal channel.

The maximal value of the non-dimensional kinetic energy of turbulence was determined for every cross-section of the boundary layer. Fig. 4a presents distributions of these maximal values versus

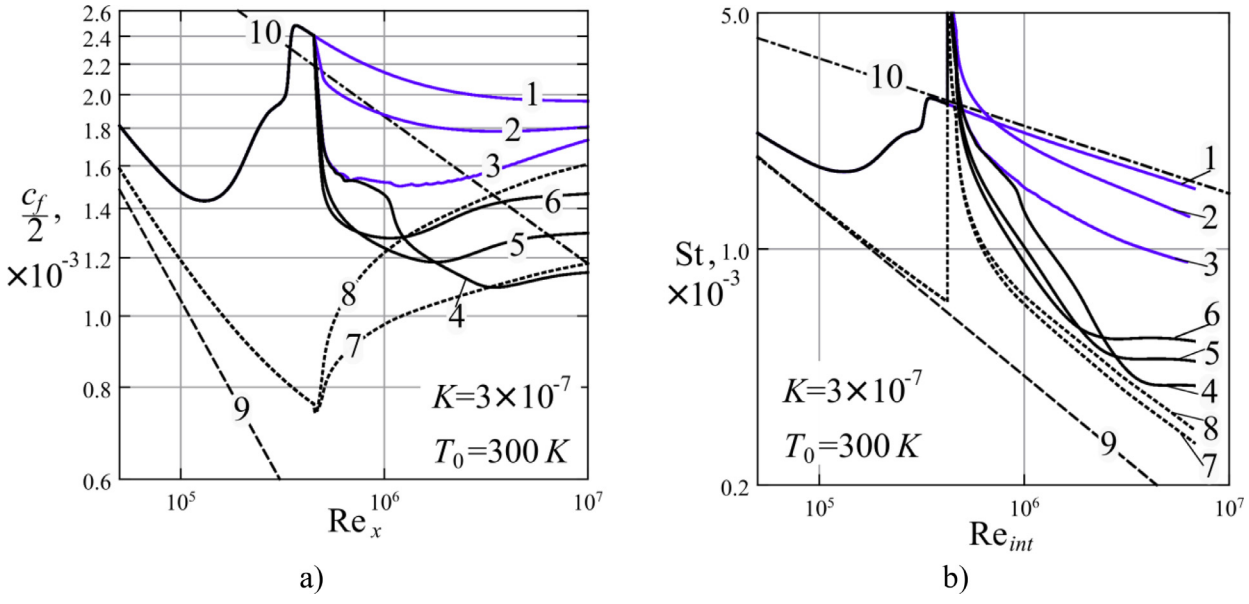

Fig. 3. Effect of wall heating on skin-friction coefficient (a) and thermal Stanton number within the accelerated boundary layer.
1 – 6 are flows with $T_w[K] = 301, 500, 1100, 1110, 1500, 2000$ respectively; 7,8 – simulations with the blocked turbulence model at $T_w[K] = 1110, 2000$ respectively; zero-pressure gradient laminar and turbulent flows: 9a – $c_f/2 = 0.332\mathrm{Re}_x^{-0.5}$, 10a – $c_f/2 = 0.0296\mathrm{Re}_x^{-0.2}$, 9b – $\mathrm{St} = 0.332\mathrm{Re}_{\mathrm{int}}^{-0.5}\mathrm{Pr}^{-2/3}$, 10b – $\mathrm{St} = 0.0296\mathrm{Re}_{\mathrm{int}}^{-0.2}\mathrm{Pr}^{-0.6}$ [39].

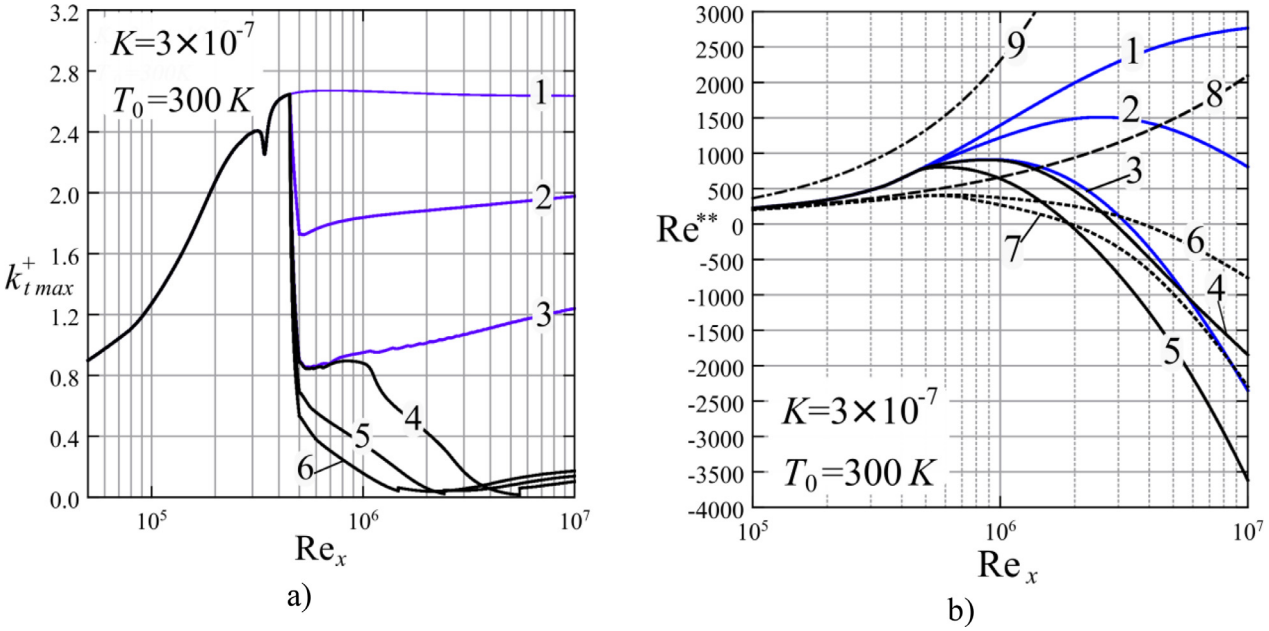

Fig. 4. a) Maximal non-dimensional kinetic energy of turbulence within the accelerated boundary layer over the heated wall, 1 – 6: see Fig. 3;
b) Local momentum thickness Reynolds number within the accelerated boundary layer over the heated wall, 1 – 5 are flows with $T_w[K] = 301, 500, 1100, 1110, 2000$ respectively; 6,7 – simulations with the blocked turbulence model at $T_w[K] = 1110, 2000$ respectively; Isothermal zero-pressure gradient flow: 8 – $\mathrm{Re}^{**} = \sqrt{0.44\mathrm{Re}_x}$(laminar), 9 – $\mathrm{Re}^{**} = 0.0366\mathrm{Re}_x^{0.8}$(turbulent).

the Reynolds number. We do not plot the maximal kinetic energy for the isothermal zero pressure gradient flow since its magnitude is about $k^+_{t\,\max} \approx 4.0$ and it worsens the clearance of lines 4 – 6. The maximal kinetic energy of turbulence goes to a certain constant value at quasi-isothermal conditions with $T_w = 301K$ (line 1). Jones et al. [44] demonstrated that in the flow with $K = 2.7 \times 10^{-7}$ streamwise turbulence intensities decrease within a certain distance from the leading edge of a convergent channel, and distributions of the intensities have no noticeable changes after this distance.

In flows with $T_w[K] = 500, 1100$ the maximal kinetic energy increases after the drop at $\mathrm{Re}_x = 5 \times 10^5$ with increase of Reynolds number. This increase of kinetic energy indicates a turbulent flow-regime but with the decreased turbulence level. At that, the increase of the wall temperature decreases the kinetic energy of turbulence.

In the flow with $T_w = 1110K$ (line 4) the maximal kinetic energy of turbulence decreases at $\mathrm{Re}_x > 10^6$ reaching zero at $\mathrm{Re}_x = 5.5 \times 10^6$. At further increase of Reynolds number the maximal kinetic energy increases slightly due to the occurrence of the second maximum in the profile of this parameter (see Fig. 12). With increase of the wall temperature (lines 5 and 6), the kinetic energy decreases in the stremwise direction more intensively than at $T_w = 1110K$. However, the kinetic energy increases with the increase of the wall temperature at $\mathrm{Re}_x = 5.5 \times 10^6 - 10^7$.

Fig. 4b shows the dependency of the local momentum thickness Reynolds number on Reynolds number based on the x-coordinate and the local velocity of the main stream. The increase of the wall temperature decreases the momentum thickness Reynolds number independently of the flow regime, presence of the local laminarization, or either working or blocked turbulence model. At $T_w = 1100$ and $\mathrm{Re}_x > 3 \times 10^6$ the momentum thickness Reynolds number takes negative values due to negative values of the momentum thickness. The formal reason of such behavior is the shape of the velocity profile with overshoot. In fact, the favorable pressure gradient and wall heating inputs additional momentum into the boundary layer that results in negative momentum thickness. We have discussed this problem in detail in work [28]. Since negative values of the momentum thickness Reynolds number take place in fully turbulent flow (line 3) then we could not apply $\mathrm{Re}^{**} = 360 - 400$ as a criterion for the direct or reverse laminar-turbulent transition in flows with the overshoot phenomenon.

It is worth noting that the local momentum thickness Reynolds number in simulations with the blocked turbulence model (lines 6, 7) is higher than one in the flows with the local laminarization (lines 4, 5) at $\mathrm{Re}_x > 3 \times 10^6$. We explain it by the higher Stanton number in flows with local laminarization than in flows simulated without turbulence model (see Fig. 3b). More intensive heat transfer facilitates the higher input of the momentum from the heated wall to the boundary layer that leads to the lower values of the momentum thickness.

Fig. 5 shows dependencies of the dimensionless thickness of the dynamic boundary layer on Reynolds number. We nondimensionalize thicknesses based on the peak value $\delta_{max} = 0.06m$ of the boundary layer thickness at quasi-isothermal conditions. Under such conditions the thickness of the dynamic boundary layer increases until $\mathrm{Re}_x < 2.7 \times 10^6$ and then decreases. Jackson et al. [45] proved experimentally such behavior of the boundary layer.

Increasing of the wall temperature (2 – 4) leads to a local drop of the boundary layer thickness at $\mathrm{Re}_x = (1.5 - 3) \times 10^6$. However, we characterize it as a formal drop since the transition to the velocity profile with overshoot takes place at the specified range of Reynolds number. Initially, the thickness of the dynamic boundary layer is defined as $U/U_e = 0.995$. The velocity maximum arises on the outer border of the layer and moves towards the wall [28]. Before this process, the velocity near the outer border increases and for some range of Reynolds number equals the velocity of the main flow. This leads to the formal drop of the boundary layer thickness. We define the thickness of the dynamic boundary layer with the velocity overshoot as $U/U_e = 1.005$.

At rather close values of the wall temperature (lines 2 and 3) but with the presence of the local laminarization at $T_w = 1110K$ the thickness of the dynamic boundary layer is only 10% less than the one of the turbulent layer. Moreover, the thickness of the boundary

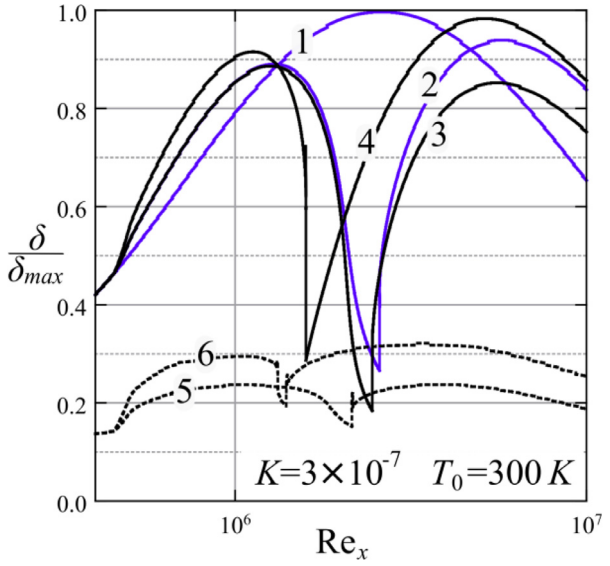

Fig. 5. Effect of wall heating on the thickness of the dynamic boundary layer with the mild pressure gradient. 1 – 4 are flows with $T_w[K] = 301, 1100, 1110, 2000$ respectively; 5, 6 – simulation with the blocked turbulence model at $T_w[K] = 1110, 2000$ respectively.

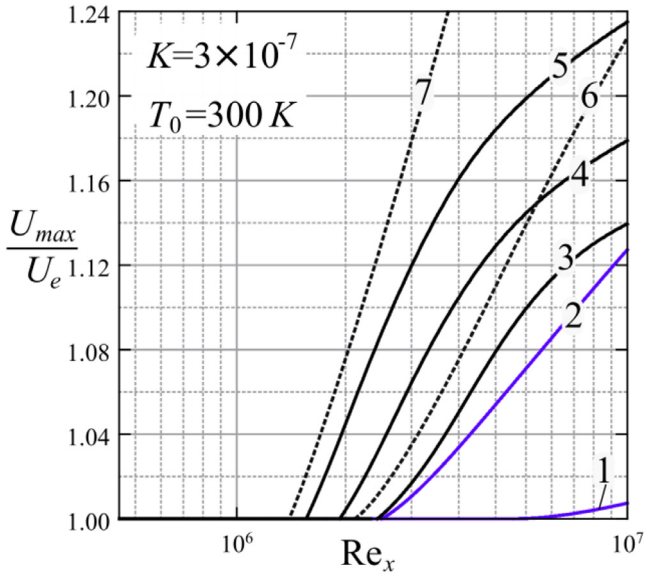

Fig. 6. Maximal velocity within the accelerated boundary layer over the heated wall. 1 – 5 are flows with $T_w[K] = 500, 1100, 1110, 1500, 2000$ respectively; 6, 7 – simulation with blocked turbulence model at $T_w[K] = 1110, 2000$ respectively.

layer over the strongly heated wall with $T_w = 2000K$ exceeds thickness of the layer in quasi-isothermal conditions at $Re_x > 4 \times 10^6$. The simulation with the blocked turbulence model (lines 5 and 6) shows significantly smaller thickness of the dynamic boundary layer than in turbulent, or laminarized flows.

Fig. 6 presents dependencies of the maximal velocity within the boundary layer on Reynolds number. The increase of wall temperature (lines 1 – 5) increases values of the maximal velocity and decreases Reynolds number at which the overshoot arises. The comparison of flows with close wall temperatures ($T_w[K] = 1100, 1110$) demonstrates that the local laminarization (line 3) facilitates the increase of maximal velocity while turbulence (line 2) reduces the velocity overshoot. The following observation supports the second statement. In flows with $T_w[K] = 1110, 1500, 2000$ the overshoot

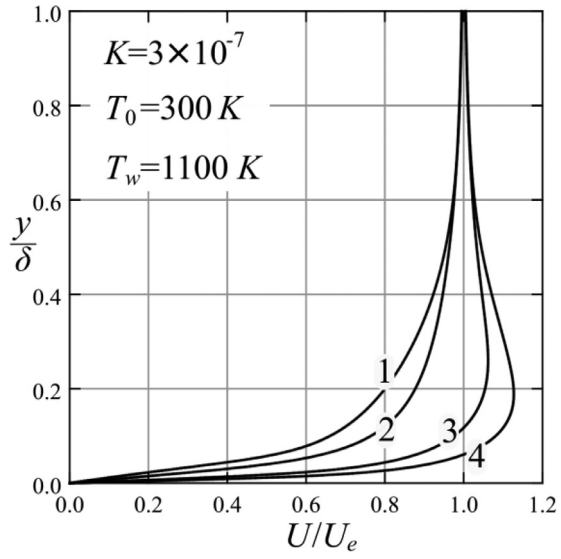

Fig. 7. Evolution of velocity profile within the accelerated boundary layer over the heated wall.
1 – 4 are cross-sections of the layer at $Re_x \times 10^{-6} = 0.5, 1, 5, 10$ respectively.

evolution is delayed at $Re_x > 7 \times 10^6$ this coincides with an arising of a second peak in the profile of the kinetic energy of turbulence (Fig. 4a).

Simulations with the blocked turbulence model (lines 6 and 7) demonstrates significantly increased maximal velocity relatively to a boundary layer with the local laminarization (lines 3 – 5). It agrees with the results of work [46], where Bryant et al. showed that the increase of the turbulence intensity decreases the magnitude of the velocity overshoot.

3.2. Local parameters for the flow at T_w=1100K

In this section we consider local characteristics of the accelerated boundary layer at the maximal wall temperature that does not lead to the arising of the local laminarization, i.e. flows keep the completely turbulent regime that is defined from a rather high level of the non-dimensional kinetic energy (Fig.4a).

Fig. 7 illustrates changes in the streamwise velocity profiles within the turbulent accelerated boundary layer over a heated wall. Velocity profiles become more filled at the beginning of the heated part of the wall ($Re_x > 5 \times 10^5 - 10^6$). The velocity profile at $Re_x = 5 \times 10^6$ already had a peak at $Re_x = 2.5 \times 10^6$ (Fig. 6). The velocity overshoot increases until the upper limit of the considered range of Reynolds number that is $Re_x = 10^7$. The overshoot in the turbulent flow has a blunt shape unlike the sharp overshoot in the laminar flow [28]. Nevertheless, the position of the overshoot moves towards the wall in a similar manner.

Fig. 8 presents distributions of the predicted intermittency factor within the accelerated boundary layer over the heated wall. It is worth being reminded of that the intermittency factor indicates a flow regime. The value of $\gamma = 0$ represents a laminar regime, while$\gamma = 1$ represents developed turbulence. The intermittency factor decreases at the beginning of the heated wall ($Re_x = 5 \times 10^5$) with a minimal value of $\gamma = 0.88$ near the wall ($y^+ = 7.8$). The factor increases with the increase of Reynolds number reaching $\gamma = 1$throughout the whole thickness of the boundary layer at $Re_x = 10^7$. Obviously, the specified minimum of the intermittency factor corresponds with the drop of the kinetic energy of turbulence in the beginning of the heated wall (Fig. 4a). Thus, the boundary layer keeps the turbulent regime at $K = 3 \times 10^{-7}$ and $T_w = 1100K$.

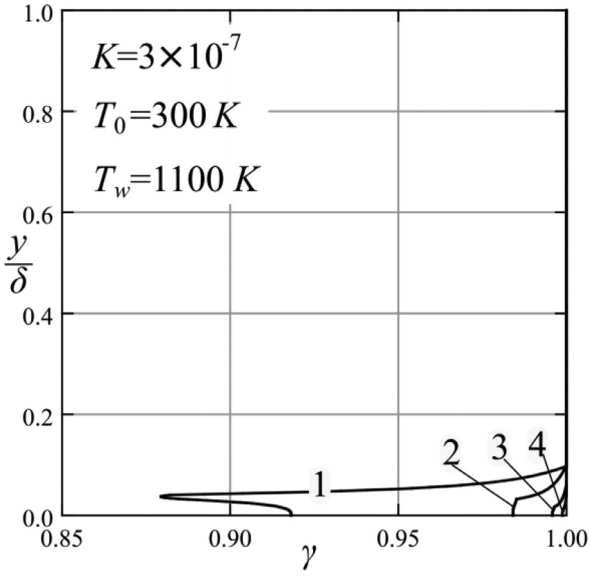

Fig. 8. Distributions of intermittency factor within the accelerated boundary layer over the heated wall. 1 – 4 – see Fig. 7.

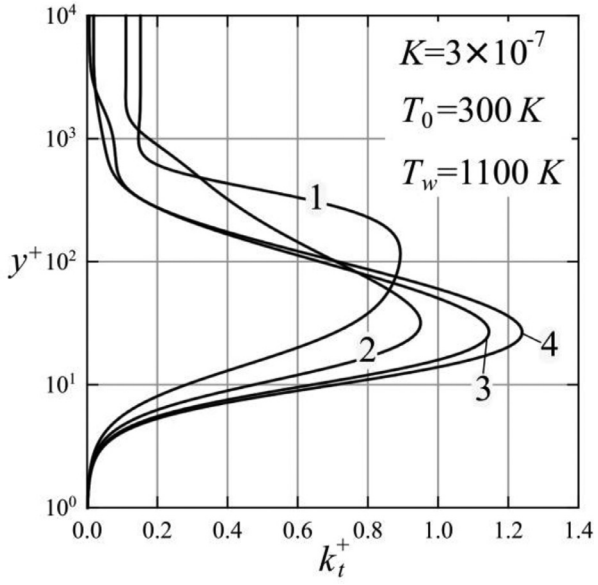

Fig. 9. Profiles of the kinetic energy of turbulence within the accelerated boundary layer over the heated wall. 1 – 4 – see Fig. 7.

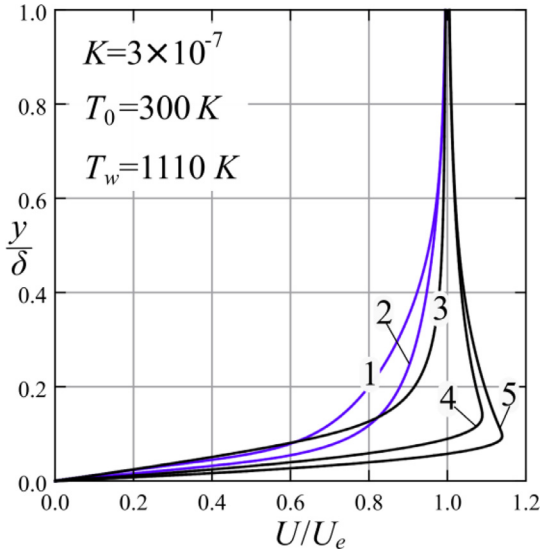

Fig. 10. Evolution of velocity profile within the accelerated boundary layer over the heated wall.
1 – 5 are cross-sections of the boundary layer at $\mathrm{Re}_x \times 10^{-6} = 0.5, 1, 2, 5, 10$ respectively.

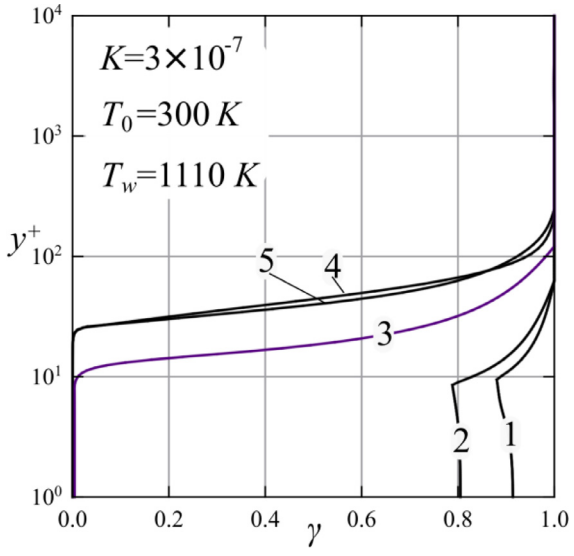

Fig. 11. Distributions of intermittency factor within the accelerated boundary layer over the heated. 1 – 5 – see Fig. 10.

Fig. 9 shows profiles of the kinetic energy of turbulence within the accelerated boundary layer over the heated wall. The profile situated in the beginning of the heated wall ($\mathrm{Re}_x = 5 \times 10^5$) keeps the shape and the position of its peak like in the developed turbulent boundary layer. Since in the present study we consider a mild pressure gradient then it has a weak influence on the flow with quasi-isothermal conditions. The profile of the kinetic energy becomes closer to the wall and increases its magnitude with increase of Reynolds number. The decrease of the boundary layer thickness explains such changes.

3.3. Local parameters for the flow at T_w=1110K

In this section we consider local characteristics of the accelerated boundary layer at the minimal wall temperature that leads to a local laminar area within the boundary layer of the present conditions.

Fig. 10 demonstrates the evolution of the streamwise velocity profiles within the boundary layer over the heated wall in the presence of the local laminarization. Profiles in the beginning of the heated wall ($\mathrm{Re}_x = 5 \times 10^5, 10^6$) have a turbulent flow and coincide with profiles 1 and 2 from Fig. 7. Moreover, the intermittency factor indicates a turbulent flow at the same Reynolds number (Fig. 11).

At $\mathrm{Re}_x = 2 \times 10^6$ the velocity profile changes its shape becoming more filled at $y/\delta > 0.16$ and decreasing the velocity gradient near the wall. The intermittency factor indicates the occurrence of the laminar area near the wall (Fig. 11). The peak arises in the velocity profile at further increase of Reynolds number. This differs from the overshoot within the turbulent boundary layer (Fig. 7) by the sharp shape and the slightly higher value of the maximal velocity.

Fig. 11 illustrates the changes of the intermittency factor within the accelerated boundary layer over the heated wall. An increase

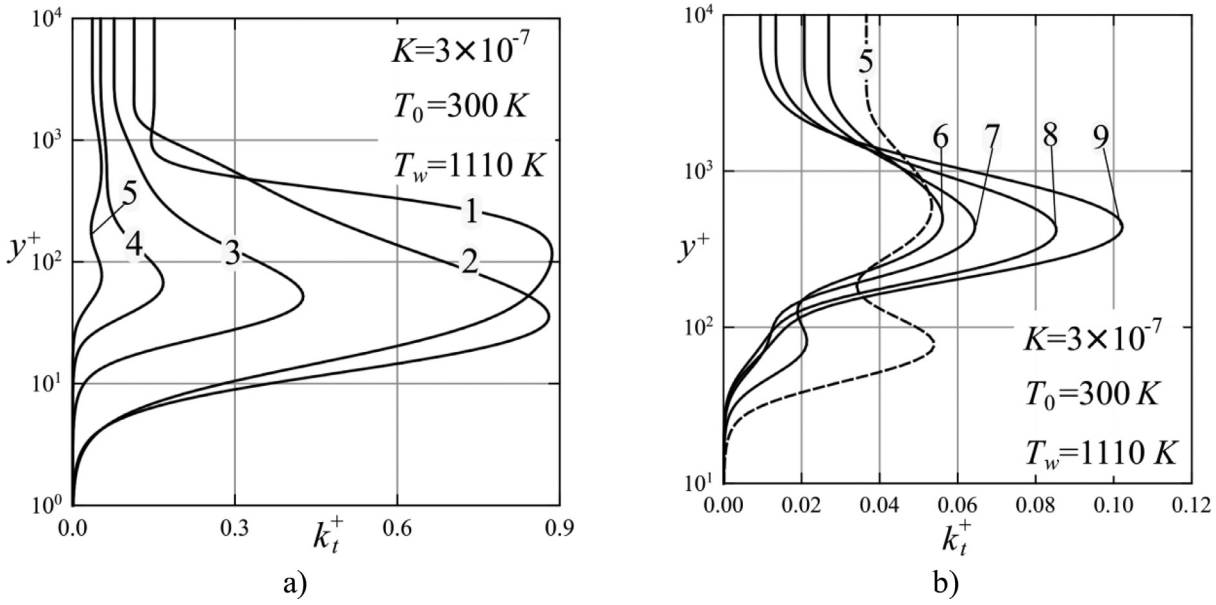

Fig. 12. Profiles of the kinetic energy of turbulence within the accelerated boundary layer over the heated wall. 1 – 9 are cross-sections of the boundary layer at $\mathrm{Re}_x \times 10^{-6} =$ 0.5, 1, 2, 3, 4, 5, 6, 8, 10 respectively.

of wall temperature from what was shown in Fig. 8. leads to a decrease in the intermittency factor. At $\mathrm{Re}_x = 10^6$ the intermittency factor has a high enough value to consider the flow turbulent. However, at $\mathrm{Re}_x = 2 \times 10^6$ the intermittency factor decreases to zero value near the wall. Thus, the local area of the laminar flow arises within the boundary layer. This area expands at $\mathrm{Re}_x = 5 \times 10^6$ and has no changes until the highest limit of $\mathrm{Re}_x = 10^7$ considered in the paper. The outer part of the boundary layer keeps the turbulent flow with $\gamma = 1$. It is worth noting that $\gamma = 1$ means a fully turbulent flow, but it does not indicate the turbulence intensity.

Fig. 12 shows distributions of the kinetic energy of turbulence within the accelerated boundary layer over the heated wall in the presence of the local laminarization. Profile 1 situated at the beginning of the heated wall ($\mathrm{Re}_x = 5 \times 10^5$) keeps the shape and the position of its peak like in a developed turbulent boundary layer. This profile coincides with profile 1 from Fig. 9. Within the considered flow with $T_w = 1110K$ the peak of the kinetic energy moves towards the wall at $\mathrm{Re}_x = 10^6$ (profile 2) and decreases up to the near complete disappearance at $\mathrm{Re}_x = 6 \times 10^6$ (profile 7).

The second peak of the non-dimensional kinetic energy of turbulence arises in the outer part of the boundary layer at $\mathrm{Re}_x = 3 \times 10^6$ (profile 4). This peak increases with the increase of Reynolds number and it keeps its position relatively close to the wall up to $\mathrm{Re}_x = 10^7$. Satake et al. [47] studied the laminarization of flow within a strongly heated circular pipe. During the suppression of turbulence, the authors obtained the behavior of velocity fluctuations similar to what is presented on Fig. 12a. Yuan and Piomelli [48, 49] have shown that peaks of the kinetic energy move away from the wall. Also, the authors support an idea that the laminarization starts near the wall.

Fig. 13 compares the comparison of the streamwise velocity profiles within the boundary layer over the heated wall with the presence of the mild pressure gradient at $\mathrm{Re}_x = 10^7$. Profile 1 corresponds the flow simulated with working turbulence model at $T_w = 1110K$. Based on the data of the intermittency factor and the kinetic energy of turbulence (Figs. 11 and 12), the near-wall part of this profile takes on laminar flow, and the other part of the profile keeps the turbulent regime. Profile 2 is simulated with the blocked turbulence model under the same conditions as profile 1. Profiles 1 and 2 coincide with each other near the wall differing with magnitude of the velocity peak.

Profile 3 was simulated with the working turbulence model at $T_w = 1100K$. It is obviously that the change of the wall temperature by 10 K at the same flow-regime is insignificant for velocity distribution within the boundary layer. However, the presence of the local laminarization near the wall leads to a noticeable difference between profiles 1 and 3 in this area. In the outer part of the boundary layer profiles 1 and 3 have the similar distribution at $y^+ > 100$(profile 1) and $y^+ > 500$ (profile 3).

Thus, profile 1 consists of the laminar and turbulent parts. In other words, the local laminarization leads to the simultaneous co-existence of the laminar and turbulent flows within the same boundary layer. Daschiel et al. [50] demonstrated co-existence of laminar and turbulent flows within a triangular duct. Authors obtained the laminarization due by decreasing the opening angle.

Fig. 14 shows a comparison between the temperature profiles within the boundary layer over the heated wall in the presence of a mild pressure gradient at $\mathrm{Re}_x = 10^7$. Temperature profiles do not have peaks, unlike velocity profiles. For this reason profiles 1 and 2 do not coincide with each other near the wall but they have the similar temperature distribution there. We explain this difference by the effect of the turbulent flow within the outer part of profile 1. This turbulent part indirectly increases the temperature gradient near the wall and, consequently, leads to a higher Stanton number than it is in the laminar flow (Fig. 3b). The thicker laminar area near the wall decreases Stanton number relative to the turbulent flow due to the lower temperature gradient than it is in the turbulent profile 3.

3.4. Local parameters for the flow at T_w=2000K

In this section we consider the local characteristics of an accelerated boundary layer with a strongly heated wall.

Fig. 15 illustrates the comparison of velocity profiles within the boundary layer over the strongly heated wall simulated with the working turbulence model (profiles 1 and 2) and with the blocked turbulence model (profiles 3 and 4). At $\mathrm{Re}_x = 10^6$ velocity profiles 1 and 3 do not have a peak, but the laminar area occurs near the

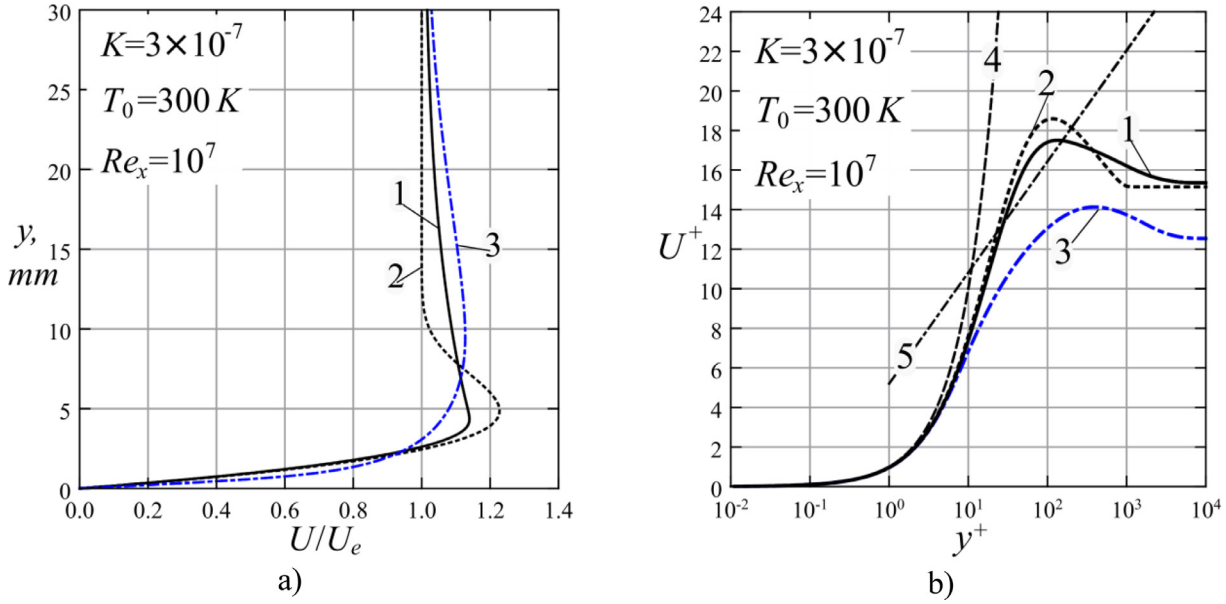

Fig. 13. Co-existence of laminar and turbulent parts of the accelerated boundary layer over the heated wall. Predicted velocity profiles at $T_w = 1110K$: 1 – simulation with working turbulence model, 2 – simulation with blocked turbulence model; 3 – predicted velocity profiles at $T_w = 1100K$, 4 – laminar sublayer $U^+ = y^+$ [39], 5 – logarithmic law $U^+ = 1/0.41ln(y^+) + 5.0$ [39].

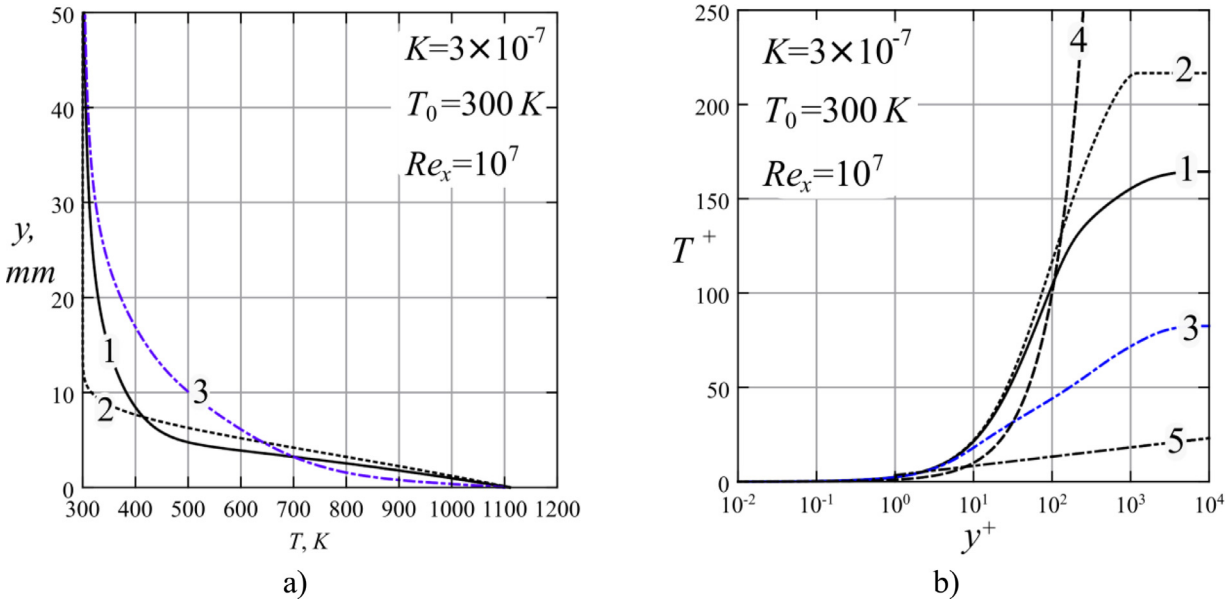

Fig. 14. Co-existence of laminar and turbulent parts of the accelerated boundary layer over the heated wall. Temperature profiles at $T_w = 1110K$: 1 – simulation with working turbulence model, 2 – simulation with blocked turbulence model; 3 – temperature profile at $T_w = 1100K$, 4 – laminar sublayer $T^+ = y^+$ [39], 5 – logarithmic law $U^+ = 1/0.47ln(y^+) + 3.48$ [39].

wall. The maximal velocity within the boundary layer at $\mathrm{Re}_x = 10^7$ simulated with the blocked turbulence model is 1.5 times higher than the velocity of the main flow. In the flow simulated with the working turbulence model under the same conditions the ratio between maximal velocity and the velocity of the main flow is 1.22. Thus, the presence of turbulent flow even at one side of the velocity peak significantly decreases the overshoot phenomenon.

Fig. 16 presents profiles of the kinetic energy of turbulence within the accelerated boundary layer over the strongly heated wall. The strong wall heating leads to the fast suppression of the initial turbulence. At that, profiles of the kinetic energy have two slight peaks, and neither of them are similar to the secondary peak at $T_w = 1110K$ (Fig. 12). The peak situated farther from the wall is suppressed faster than the peak near the wall. In the flow with $T_w = 2000K$ the kinetic energy of turbulence reaches near-zero values at $\mathrm{Re}_x = 2 \times 10^6$. After this, the secondary peak of the kinetic energy arises and increases. Its value at $\mathrm{Re}_x = 10^7$ is 1.5 times higher than one in the flow with $T_w = 1110K$ (Fig. 12) but it is still smaller than the kinetic energy in a fully developed turbulent boundary layer.

It is worth noting that there is a positive correlation between the magnitude of the velocity overshoot and the increase of the secondary arised peak of the kinetic energy of turbulence. It may have the following explanation. The velocity within the boundary layer significantly exceeds the velocity of the main flow. It initiates shear layers that generate the secondary peak of tur-

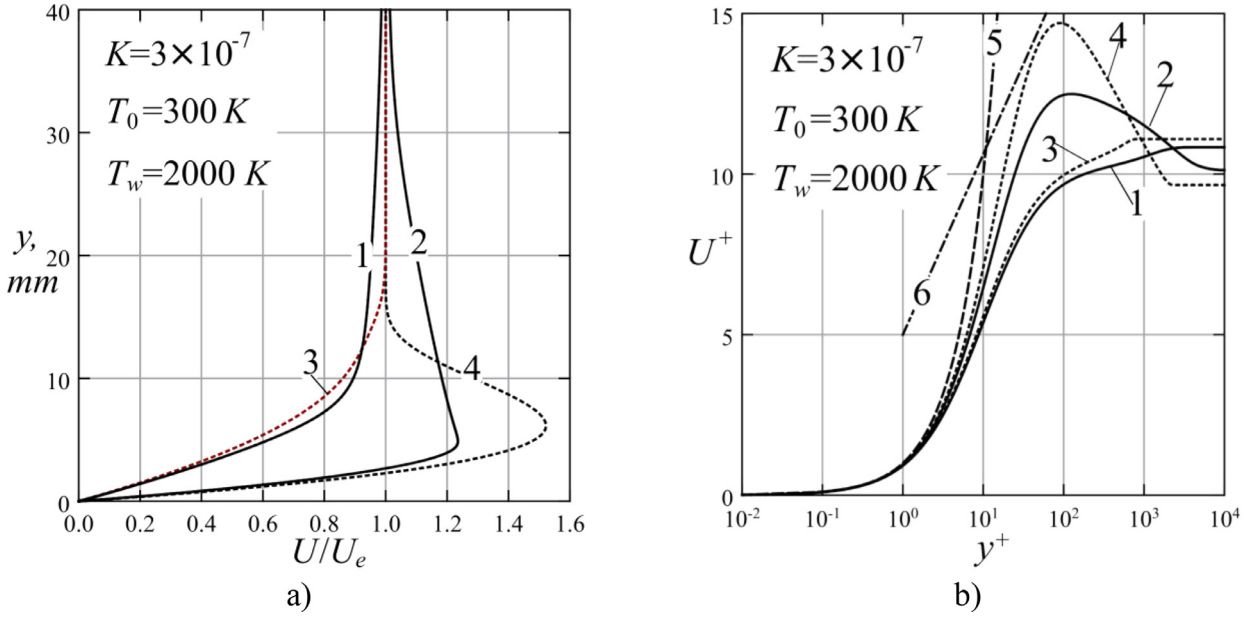

Fig. 15. Effect of turbulence on velocity profiles within the accelerated boundary layer over the strongly heated wall. Simulation with working turbulence model: 1, 2 – $Re_x = 10^6, 10^7$ respectively; Simulation with blocked turbulence model: 3, 4 – $Re_x = 10^6, 10^7$ respectively, 4 – laminar sublayer $U^+ = y^+$ [39], 5 – logarithmic law $U^+ = 1/0.41ln(y^+) + 5.0$ [39].

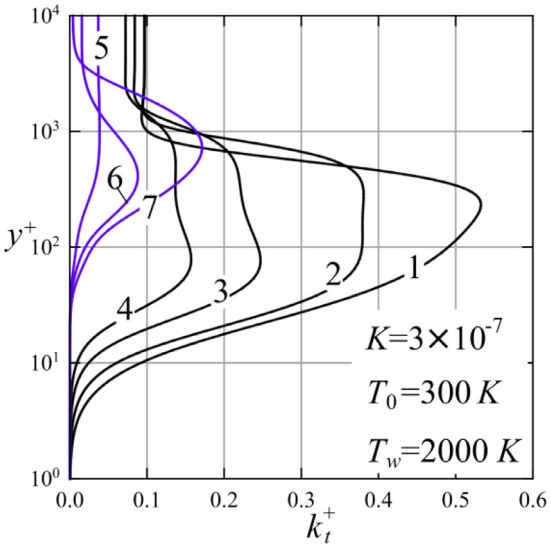

Fig. 16. Profiles of kinetic energy of turbulence within the accelerated boundary layer over the strongly heated wall.
1 – 7 are cross-sections of the boundary layer at $Re_x \times 10^{-6} = 0.5, 0.6, 0.8, 1, 2, 4, 10$ respectively.

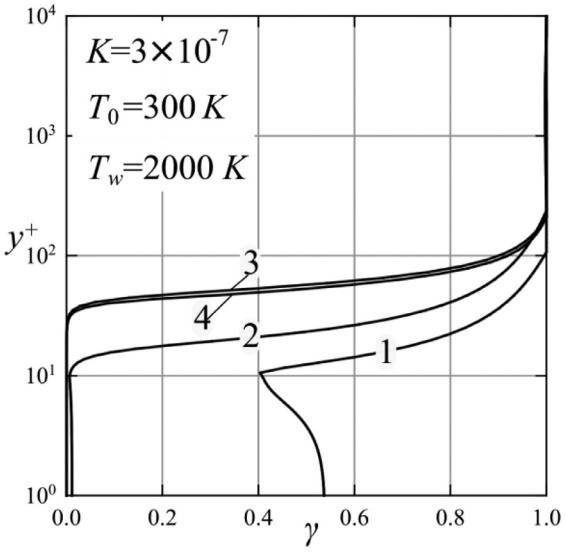

Fig. 17. Distributions of intermittency factor within the accelerated boundary layer over the strongly heated. 1 – 4 are cross-sections of the boundary layer at $Re_x \times 10^{-6} = 0.5, 1, 5, 10$ respectively.

bulence. Thus, the velocity overshoot suppresses the turbulence near the wall, but at the same time it generates a new source of the turbulence between the velocity maximum and the potential flow.

Fig. 17 shows distributions of the intermittency factor within the accelerated boundary layer over the strongly heated wall. In this flow-case the intermittency factor decreases noticeably near the surface in the beginning of the heated wall at $Re_x = 5 \times 10^5$, and the laminar area occurs at $Re_x = 10^6$ which is lower a value than in the flow with $T_w = 1110K$. The strong heating of the wall slightly increases the area of the local laminarization ($\gamma \approx 0$) over the thickness of the boundary layer at $Re_x = 5 \times 10^6 - 10^7$.

4. Conclusions

The paper presents numerical study of the air flow over the heated wall with the presence of the mild favorable pressure gradient. It was found that under such conditions, laminar flow may arise in the near-wall region of the boundary layer. The investigation has the following results:

– Despite the mild favorable pressure gradient the wall heating leads to the occurrence of the velocity overshoot due to the decrease of the air density near the wall. These velocity peaks increases their values in streamwise direction, this leads to additional acceleration near the wall. This acceleration suppresses the turbulence.

- On the one hand, the local laminarization leads to a significant decrease of the skin-friction coefficient to the values of the laminar boundary layer at the same flow acceleration and the temperature difference between the wall and the main flow. On the other hand, the velocity overshoot increases the skin-friction coefficient due to the increase of the normal velocity gradient near the wall. Nevertheless, the suppression of the turbulence prevails over the direct effect of the velocity overshoot.
- The decrease of the turbulence intensity significantly decreases the Stanton number. This parameter could reach the value of the laminar flow in the presence of the local laminarization. However, the arising of the velocity overshoot generates a secondary peak of the kinetic energy of turbulence between the velocity maximum and the main flow. This secondary turbulence increases the normal temperature gradient within the near-wall laminarized area and also slightly increases the Stanton number. At that, Stanton number keeps an approximately constant value with an increase of the integral Reynolds number and increases with an increase of the temperature difference between the wall and the main flow.
- The local laminarization has a weak effect on the thickness of the dynamic boundary layer (about 10 – 15%). The thickness has the same order of the magnitude as one in the accelerated turbulent flow at quasi-isothermal conditions.
- Generally, the velocity overshoot and turbulence look like phenomena opposite to each other. The turbulence decreases the magnitude of the overshoot and changes the peak of velocity to a blunt shape. In its turn, the velocity overshoot suppresses the turbulence in the near-wall region of the boundary layer. However, at the same time the overshoot correlates with the secondary turbulization of the flow in the outer part of the boundary layer. The problem of this correlation needs an additional study.
- In the presence of the local laminarization the profile of the streamwise velocity consists of the completely laminar part, situated between the velocity peak and the wall, and the turbulent part, placed between the velocity peak and the main flow. The temperature profile consists of laminar part and turbulent one as well. The flow regimes for each part of the boundary layer was uniquely identified on the basis of the intermittency factor.
- The increase of the wall temperature in the considered conditions decreases the Reynolds number (Re_x), at which the velocity overshoot and laminarized area arise within the boundary layer.

Thus, the considered flow conditions may result in a boundary layer consisting of a near-wall laminar part and an outer turbulent one. Such character of the flow leads to levels of friction and heat transfer intermediate to laminar and turbulent flow at the same conditions. The skin-friction coefficient in a turbulent simulation may be slightly lower than one in the boundary layer simulated without turbulence model but at the same other conditions. In that case, we may say that the presence of turbulence is able to decrease the friction.

5. Author declaration

We wish to confirm that there are no known conflicts of interest associated with this publication “Local Laminarization within the Mild Pressure Gradient Flow over the Heated Wall” and there has been no significant financial support for this work that could have influenced its outcome.

We confirm that the manuscript has been read and approved by all named authors and that there are no other persons who satisfied the criteria for authorship but are not listed. We further confirm that the order of authors listed in the manuscript has been approved by all of us.

We confirm that we have given due consideration to the protection of intellectual property associated with this work and that there are no impediments to publication, including the timing of publication, with respect to intellectual property. In so doing we confirm that we have followed the regulations of our institutions concerning intellectual property.

We understand that the Corresponding Author (Dr. Alexey Sakhnov) is the sole contact for the Editorial process (including Editorial Manager and direct communications with the office). He is responsible for communicating with the other authors about progress, submissions of revisions and final approval of proofs. We confirm that we have provided a current, correct email address which is accessible by the Corresponding Author (Dr. Alexey Sakhnov) and which has been configured to accept email from aleksei_sakhnov@mail.ru.

Declaration of Competing Interest

The authors declare that they have no known competing financial interests or personal relationships that could have appeared to influence the work reported in this paper.

Acknowledgments

The author acknowledges Sidney D.V. Williams from Georgia Institute of Technology (Atlanta, US) for his corrections of the paper’s text.

References

[1] M.E. Deich, A.A. Koh, A.V. Robozhev, V.F. Stepanchuk, Investigation of the flow structure in ejector stage with the isobaric initial mixing section, Therm. Eng. 12 (1954) 24–32 (in Russian).
[2] J. Sternberg, Transition From A Turbulent To Laminar Boundary Layer, U.S. Army Ballistics Research lab, Aberdeen, 1954 Rept No. 906.
[3] D.G. Wilson, S.A. Pope, Convective heat transfer to gas turbine blade surfaces, Proc. Instn. Mech. Engrs. Lond 168 (1954) 861.
[4] R. Narasimha, K.R. Sreenivasan, Relaminarization fluid flows, Adv. Appl. Mech. 19 (1979) 221–309.
[5] A.V. Dovgal, V.Ya. Levchenko, V.A. Timofeev, Boundary layer control by a local heating of the wall, IUTAM symposium toulouse, France (1) 1989. – Laminar-Turbulent Transition, Arnal D., Michel R. (Editors). p. 113–121.
[6] S.L. Chernyshev, A.Ph. Kiselev, A.P. Kuryachii, Laminar flow control research at TsAGI: past and present, Prog. Aerosp. Sci. 47 (2011) 169–185.
[7] G.R. Grek, V.V. Kozlov, M.P. Ramazanov, Investigation of boundary layer stability in a gradient flow with a high degree of free-stream turbulence, Fluid Dyn. 25 (1990) 207–213 https://doi.org/10.1007/BF01058969.
[8] V.V. Kozlov, V. Ya. Levchenko, V.A. Sova, V.A. Shcherbakov, Acoustic field effect on laminar turbulent transition on a swept wing in the favorable pressure gradient region, Fluid Dyn. 38 (2003) 868–877 https://doi.org/10.1023/B:FLUI.0000015227.07480.fa.
[9] G.R. Grek, M.M. Katasonov, V.V. Kozlov, Modelling of streaky structures and turbulent-spot generation process in wing boundary layer at high free-stream turbulence, Thermophys. Aeromech 15 (2008) 549–561 https://doi.org/10.1007/s11510-008-0003-5.
[10] K.R. Sreenivasan, Laminarescent, relaminarizing and retransitional flows, Acta Mech. 44 (1982) 1–48.
[11] M.A. Badri Narayanan, V. Ramjee, On the criteria for reverse transition in a two-dimensional boundary layer flow, J. Fluid Mech. 35 (2) (1969) 225–241, doi:10.1017/S002211206900108X.
[12] B.E. Launder, Laminarization of the turbulent boundary layer in a severe acceleration, J. Appl. Mech. 31 (4) (1964) 707–708.
[13] W.M. Kays, Convective Heat and Mass Transfer, McGraw-Hill, New York, 1966.
[14] C. Bourassa, F.O. Thomas, An experimental investigation of a highly accelerated turbulent boundary layer, J. Fluid Mech. 634 (2009) 359–404.
[15] Sh.A. Dixit, O.N. Ramesh, Large-scale structures in turbulent and reverse-transitional sink flow boundary layers, J. Fluid Mech. 649 (2010) 233–273, doi:10.1017/S0022112009993430.
[16] G. Araya, G. Torres, Structural Reynolds analogy in laminarescent boundary layers via DNS, J. Visual. 22 (2019) 529–540 https://doi.org/10.1007/s12650-019-00549-6.
[17] V.G. Lushchik, M.S. Makarova, A.I. Reshmin, Laminarization of Flow with Heat transfer in a plane channel with a confuser, Fluid Dyn. 54 (2019) 67–76 https://doi.org/10.1134/S0015462819010099.

[18] G. Saltar, G. Araya, Reynolds shear stress modeling in turbulent boundary layers subject to very strong favorable pressure gradient, Comput. Fluids 202 (2020) 104494 https://doi.org/10.1016/j.compfluid.2020.104494.
[19] D.P. Mikielewicz, A.M. Shehata, J.D. Jackson, D.M. McEligot, Temperature, velocity and mean turbulence structure in strongly heated internal gas flows. Comparison of numerical predictions with data, Int. J. Heat Mass Transf. 45 (2002) 4333–4352.
[20] D.M. McEligot, Xu Chu, R.S. Skifton, E. Laurien, Internal convective heat transfer to gases in the low-Reynolds-number "turbulent" range, Int. J. Heat Mass Transf. 121 (2018) 1118–1124 https://doi.org/10.1016/j.ijheatmasstransfer.2017.12.086.
[21] T. Takagi, H.-D. Shin, A. Ishio, Local laminarization in turbulent diffusion flames, Combust. Flame 37 (1980) 163–170.
[22] M. Hadžiabdić, K. Hanjalić, R. Mullyadzhanov, LES of turbulent flow in a concentric annulus with rotating outer wall, Int. J. Heat Fluid Flow 43 (2013) 74–84 http://dx.doi.org/10.1016/j.ijheatfluidflow.2013.05.008.
[23] N. Shiibara, H. Nakamura, Sh. Yamada, Unsteady characteristics of turbulent heat transfer in a circular pipe upon sudden acceleration and deceleration of flow, Int. J. Heat Mass Transf. 113 (2017) 490–501 http://dx.doi.org/10.1016/j.ijheatmasstransfer.2017.05.077.
[24] N.I. Mikheev, I.I. Saushin, A.E. Goltsman, Phase evolution of terms of turbulent kinetic energy transport equation in the boundary layer of a pulsating flow, IOP Conf. Series, J. Phys. 1105 (2018) 012025, doi:10.1088/1742-6596/1105/1/012025.
[25] J. Kühnen, D. Scarselli, M. Schaner, B. Hof, Relaminarization by steady modification of the streamwise velocity profile in a pipe, Flow Turbul. Combust. 100 (2018) 919–943 https://doi.org/10.1007/s10494-018-9896-4.
[26] B.F. Boyarshinov, E.P. Volchkov, V.V. Lukashov, Heat transfer in accelerated chemically reacting boundary layer, Dokl. Akad. Nauk 350 (6) (1996) 763–765 (in Russian).
[27] E.P. Volchkov, Concerning the heat and mass transfer features on permeable surfaces, Int. J. Heat Mass Transf. 49 (3-4) (2006) 755–762.
[28] A.Yu. Sakhnov, Evolution of accelerated laminar boundary layer subjected to isothermal wall heating, Int. J. Heat Mass Transf. 82 (2015) 348–356 http://dx.doi.org/10.1016/j.ijheatmasstransfer.2014.11.068.
[29] A.Yu. Sakhnov, Effect of gas properties on accelerated laminar boundary layer over a heated wall, Int. J. Heat Mass Transf. 111 (2017) 1121–1128 https://doi.org/10.1016/j.ijheatmasstransfer.2017.04.089.
[30] A.Yu. Sakhnov, Influence of thermal conditions on accelerated boundary layer subjected to a wall heating, AIP Conf. Proc. 1648 (ICNAAM14) (2015) 850068 http://dx.doi.org/10.1063/1.4913123.
[31] A.Yu. Sakhnov, Numerical simulation of helium injection into the accelerated turbulent xenon flow, IOP Conf. Series, J. Phys. 1105 (2018) 012013–012016, doi:10.1088/1742-6596/1105/1/012013.
[32] R.J. Moffat, W.M. Kays, A review of turbulent boundary layer heat transfer research at Stanford 1958–1983, Adv. Heat Transf. 16 (1984) 242–365.
[33] B.J. McBride, S. Gordon, Computer Program for Calculation of Complex Chemical Equilibrium Compositions and Applications, 1311, Part II Users manual and program description // NASA reference publication, 1996 June.
[34] L. Wei, X. Ge, J. George, P. Durbin, An intermittency transport model for transitional flows on smooth and rough walls, ERCOFTAC Bull. 106 (2016) 54–59.
[35] X. Ge, S. Arolla, P. Durbin, A bypass transition model based on the intermittency function, Flow Turbul. Combust. 93 (2014) 37–61, doi:10.1007/s10494-014-9533-9.
[36] A.D. Anderson, J.C. Tannehill, R.H. Pletcher, Computational Fluid Mechanics and Heat Transfer, Hemisphere Publishing Corporation, New York, 1984.
[37] A.Yu. Sakhnov, Accelerated laminar flow near the heated permeable surface, Int. J. Heat Mass Transf. 127 (Part B) (2018) 17–24.
[38] H.L. Julien, W.M. Kays, R.J. Moffat, The Turbulent Boundary Layer On A Porous Plate: Experimental Study Of The Effects Of A Favorable Pressure Gradient, Rept No. HMT-4, Stanford University, Dept. of Mech. Eng., CA, 1969.
[39] H. Schlichting, K. Gersten, Boundary Layer Theory, eighth ed., Springer, Berlin, 2003.
[40] E. Ghasemi, D.M. McEligot, K. Nolan, J. Crepeau, A. Siahpush, R.S. Budwig, Effects of adverse and favorable pressure gradients on entropy generation in a transitional boundary layer region under the influence of freestream turbulence, Int. J. Heat Mass Transf. 77 (2014) 475–488.
[41] E. Ghasemi, D.M. McEligot, K.P. Nolan, J. Crepeau, A. Tokuhiro, R.S. Budwig, Entropy generation in a transitional boundary layer region under the influence of freestream turbulence using transitional RANS models and DNS, Int. Commun. Heat Mass Transf. 41 (2013) 10–16 http://dx.doi.org/10.1016/j.icheatmasstransfer.2012.11.005.
[42] E.P. Volchkov, M.S. Makarov, A.Yu. Sakhnov, Heat transfer in the boundary layer with asymptotic favorable pressure gradient, Int. J. Heat Mass Transf. 55 (4) (2012) 1126–1132.
[43] B. Shome, Numerical study of turbulent flow in asymmetrically heated horizontal channel, Int. J. Therm. Sci. 103 (2016) 10–23 http://dx.doi.org/10.1016/j.ijthermalsci.2015.12.010.
[44] M.B. Jones, I. Marusic, A.E. Perry, Evolution and structure of sink-flow turbulent boundary layers, J. Fluid Mech. 428 (2001) 1–27.
[45] R.B. Jackson, B.G. Woods, W.R. Marcum, Boundary layer laminarization by convex curvature and acceleration, Nucl. Eng. Des. 278 (2014) 693–700 http://dx.doi.org/10.1016/j.nucengdes.2014.07.020.
[46] D.B. Bryant, E.M. Sparrow, J.M. Gorman, Turbulent pipe flow in the presence of centerline velocity overshoot and wall-shear undershoot, Int. J. Therm. Sci. 125 (2018) 218–230 https://doi.org/10.1016/j.ijthermalsci.2017.11.028.
[47] S. Satake, T. Kunugi, A.M. Shehata, D.M. McEligot, Direct numerical simulation for laminarization of turbulent forced gas flows in circular tubes with strong heating, Int. J. Heat Fluid Flow 21 (2000) 526–534.
[48] J. Yuan, U. Piomelli, Numerical simulations of sink-flow boundary layers over rough surfaces, Phys. Fluids 26 (2014) 015113 https://doi.org/10.1063/1.4862672.
[49] J. Yuan, U. Piomelli, Numerical simulation of a spatially developing accelerating boundary layer over roughness, J. Fluid Mech. 780 (2015) 192–214, doi:10.1017/jfm.2015.437.
[50] G. Daschiel, B. Frohnapfel, J. Jovanović, Numerical investigation of flow through a triangular duct: The coexistence of laminar and turbulent flow, Int. J. Heat Fluid Flow 41 (2013) 27–33 http://dx.doi.org/10.1016/j.ijheatfluidflow.2013.03.016.